JOURNAL OF AIRCRAFT
Vol. 45, No. 5, September–October 2008

Flow Control for the Systematic Buildup of High-Lift Systems

Arvin Shmilovich* and Yoram Yadlin†
The Boeing Company, Huntington Beach, California 92647

DOI: 10.2514/1.35327

Enhanced high-lift airplane performance using active flow control is investigated. A computational fluid dynamics process has been developed for flow simulations in conjunction with active control. The analysis tool has been validated with experimental data and it has been extensively used to gain insight into high-lift flows that are subject to various modes of actuation. The computational method has been used for a methodical buildup of distributed flow control systems with substantial gains in aerodynamic efficiency. The versatility of the distributed active flow control offers a high payoff for the practical airframe integration of high-lift systems.

Nomenclature

C_D	=	drag coefficient
C_L	=	lift coefficient
$C_{L\,\max}$	=	maximum lift coefficient
C_p	=	pressure coefficient
C_μ	=	slot momentum coefficient, $(h/c) \cdot (\rho_j/\rho_\infty) \cdot (U_j/U_\infty)^2$
c	=	chord length
F^+	=	reduced forcing frequency, $f \cdot c/U_\infty$
f	=	actuator frequency, Hz
h	=	actuator slot width
L/D	=	lift-to-drag ratio
U_j/U_∞	=	ratio of jet actuator peak velocity to freestream velocity
u_x	=	streamwise component of the velocity vector
α	=	angle of attack
δ_{flap}	=	flap deflection angle
ρ_j/ρ_∞	=	ratio of jet actuator density to freestream density

I. Introduction

TAKEOFF and landing performance are two of the principal design objectives of transport airplanes. Any airplane design is limited to a maximum takeoff weight, which is related to the runway length. For a given runway length, higher lift levels permit a larger airplane weight. Equivalently, for a given weight, higher lift allows for a lower stall speed and a shorter runway. From an operational perspective, this translates into access to a larger number of airports. Whether the requirement is for a higher airplane weight or for shorter runways, superior high-lift capability is a key design objective of the airplane manufacturers.

Efficient high-lift systems provide crucial performance advantages for both military and commercial airplanes. In the context of military airplanes, an area of high priority is the ability to operate off remote and austere fields. Military transports with short runway capability are essential for maximizing the global reach of the airlift force. With respect to commercial transports, the economic impact of high-lift systems is substantial. A set of trade factors described by Garner et al. [1] is used to illustrate these advantages. For example, an increase in the aircraft maximum lift coefficient results in a larger payload for a fixed approach speed. Similarly, an increase in the takeoff lift-to-drag ratio (L/D) results in a larger payload or a longer range. Also, a gain in the lift coefficient at a constant angle of attack reduces the approach attitude, allowing for a shortened landing gear with a corresponding reduction in aircraft weight.

Another aspect of the economic advantage attributable to enhanced high-lift capability relates to environmental regulations. A growing number of communities enforce stringent noise limits in airport environments, resulting in limited hours of operation. Moreover, aircraft that do not operate within the permissible noise limits are financially penalized or even prohibited from operating in and out of certain airports. For example, to comply with environmental regulations, some aircraft have been forced to reduce payload, as well as reduce takeoff and liftoff speeds during the initial climb. However, with fewer passengers on board, operating the aircraft becomes economically inviable. Consequently, there is a great economic incentive to develop aircraft with improved takeoff and landing performance.

The aerodynamic design is especially challenging for takeoff and landing conditions in which the fluid flow is dominated by viscous effects. Techniques for altering the viscous flow structures at these high-lift conditions are highly desirable due to the increased potential for improved efficiency. A variety of flow control applications based on active systems have been investigated in recent years [2–9]. Several studies were aimed at improving the performance of airfoils at high incidence by addressing the problem of leading-edge separation [10–15]. In another set of studies, active flow control (AFC) has been applied to enhance the high-lift performance of airfoils with deflected slats and flap elements [16–19]. Although these investigations demonstrate various degrees of performance improvements, the question of whether the gains are substantial enough to warrant the development of a whole new airplane using AFC technology is still unanswered. The objective of the current study is to explore ways of implementing AFC to provide very high levels of performance while addressing issues of practical airframe integration.

In the following sections, a brief review of the numerical procedure developed for the high-lift problem within the framework of time-dependent modeling of the AFC is presented. This will be followed by a validation of the numerical scheme using experimental data obtained for a wing mounted between two walls. The rationale for developing a distributed AFC system will be discussed, and aerodynamic performance goals will be established. Results of sample simulations will be presented, with emphasis on the flow diagnostics used for establishing the efficacy of the distributed flow control approach. The paper will conclude with a discussion on aspects of practical airframe integration of flow control systems.

II. Numerical Procedure

The numerical tool used for the simulation of high-lift configurations within the context of the AFC is a modified version

Presented as Paper 2855 at the 3rd AIAA Flow Control Conference, San Francisco, CA, 5–8 June 2006; received 5 November 2007; accepted for publication 18 November 2007.

*Technical Fellow, Aerodynamic Technology, 5301 Bolsa Avenue, M/S H013-B308. Senior Member AIAA.

†Senior Engineer/Scientist, Aerodynamic Technology, 5301 Bolsa Avenue, M/S H013-B308. Senior Member AIAA.

of the OVERFLOW code originally developed by NASA (Buning et al [20]). OVERFLOW uses the unsteady Reynolds-averaged Navier–Stokes formulation for overset grid systems. The numerical procedure has been modified to facilitate the development of various flow control techniques.

Special modules have been developed for the modeling of time-varying boundary conditions to simulate the flow excitation due to the control devices. Jet actuation is defined by the mass flow rate, the cross-sectional area, and the stagnation pressure and temperature to determine the velocity at the actuator nozzle. The numerical algorithm uses the characteristics approach for the consistent application of the boundary conditions.

In the case of pulsed jets, the flux vector is aligned with the nozzle axis, and jet pulsation is determined by a forcing frequency. Various signal shapes ranging from sinusoidal to step function (i.e., jet velocity as a function of time) are defined by sets of analytical functions with continuous first and second derivatives.

The calculations were obtained using a second-order upwind differencing scheme and the Spalart–Allmaras turbulence model. The flow control computations use a second-order time-accurate scheme with 800 time steps per actuation cycle. The calculation is initiated from a steady-state solution obtained for the flow in the absence of any actuation. Limit-cycle convergence is achieved after approximately 50 actuation cycles.

III. Validation with Experimental Data

High-lift systems that consist of simple hinge moveable elements are very attractive because they are lighter and mechanically simpler than slotted multi-element systems, resulting in a lower manufacturing cost. The aerodynamic characteristics of simple hinge systems are not as good as slotted wing sections, and the objective is to augment their performance using the AFC. The validation of the current computational method for AFC applications has been performed for a set of wing sections with simple hinge elements that have been tested by Kiedaisch et al. [19] at the Illinois Institute of Technology. The models were mounted between two side walls where the objective was to obtain two-dimensional flow characteristics. Two-dimensional flow simulations for airfoil sections in free air were used in this study. Figure 1 shows the grid topology used for a section with a 15 deg droop leading edge and a simple hinge flap with a 25 deg deflection. The mesh consists of three overlapping systems. The flow control device is represented by a nozzle having a constant cross-sectional area embedded within the airfoil at the flap hinge line. The nozzle area and its orientation are consistent with the area and the angle of the actuator at the exit station in the experimental setup. An additional C-type mesh is used to capture the flow features in the vicinity of the sharp edge defined by the nozzle and the airfoil contour.

The first solution is obtained for a freestream Mach number of 0.09, an angle of attack of 11 deg, and a chord Reynolds number of 0.75×10^6. Initially, a steady-state solution for the fully attached flow is obtained for the baseline case without flow control actuation. At the 3000th time step, flow control is activated with a frequency of 217 Hz (an F^+ of 2.56) and a momentum coefficient C_μ of 0.015, corresponding to a jet maximum velocity of 2.5 times the freestream velocity. The actuation signal is shown in the inset of Fig. 2. The development of the forces on the airfoil, shown in Fig. 2, indicates that limit cycle is obtained after approximately 40 actuation cycles. The short time-scale flow characteristics in the aft portion of the airfoil, once the limit cycle has been achieved, are shown in Fig. 3. The baseline flow with a very large flow separation bubble in the wake of the flap is also shown for reference. The snapshots show instantaneous contours of the streamwise component of the velocity u_x, in which the yellow-red color bands represent flow reversal. Separated flow is indicative of an aerodynamic deficiency in the form of reduced lift and increased drag. Each plot includes a graph of the periodic flux at the individual ports. The unsteady flow excitation is described by the loci of particles continuously released from a vertical rake located upstream of the hinge line over a time interval corresponding to two actuation cycles (~0.01 s). The calculation

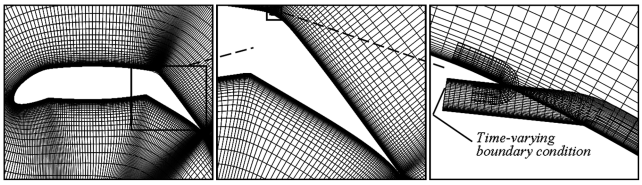

Fig. 1 Grid topology for the flow control application.

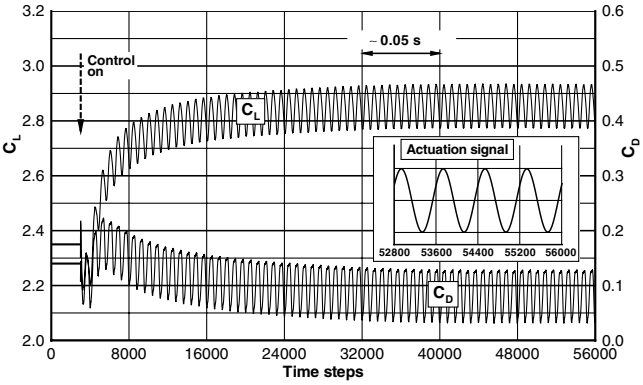

Fig. 2 Force development due to actuation for $\delta_{\text{flap}} = 25$ deg, $\alpha = 11$ deg.

indicates that in a time-average sense the intermittent ejection is quite effective in attaching the flow. The flow is streamlined in the hinge line region and flow separation is confined to the aft portion of the flap.

The next set of results is obtained for the single- and two-element slotted-slat configurations with 40 deg flap deflections. A flow control with a momentum coefficient of 0.015 and a frequency of 90 Hz (an F^+ of 1.06) is used. The computed flowfield for the single-element section is shown in Fig. 4, demonstrating that the AFC is quite beneficial even for cases where the flow is massively separated. A comparison with experimental data in terms of time-averaged lift and pressure distributions is shown in Figs. 5 and 6, respectively. Good agreement is obtained in the linear range of the angles of attack for both the baseline and the flow actuated cases. However, major discrepancies exist at the $C_{L\,\max}$ conditions. There are several sources of inconsistencies that might explain the poor agreement at the high-flow incidence. From the experimental standpoint, because there was no side wall boundary layer treatment, the separation pattern at the large incidence was most likely contaminated by the separation of the viscous layers of the side walls. This effect is particularly detrimental for the small span-to-chord ratio of 1.57 in this experiment. With respect to the flow analysis, the computational tool is not accurate at $C_{L\,\max}$ conditions due to shortcomings in the turbulence modeling. Another source of inconsistency is the AFC application, in which the sinusoidal actuation signal prescribed in the simulations is not identical to the experiment. In view of these uncertainties, the computational predictions are quite encouraging, especially in the linear range. Because lift augmentation due to the AFC is reasonably well captured, the analysis tool will be used next for developing more practical AFC implementations with higher aerodynamic efficiency.

A different method for the calculation of AFC flows based on unstructured grid topologies was used by Galbraith [21]. However, predicted lift increments due to flow control for the same airfoil used in the current study have not shown satisfactory agreement with the experiment.

IV. Distributed Flow Control

In reviewing the results presented in Figs. 3–6, it is clear that the actuation at the hinge point is effective. It is also conceivable that additional lift can be achieved if the flow quality in the aft portion of the flap could be further improved. The lift coefficient for the single-

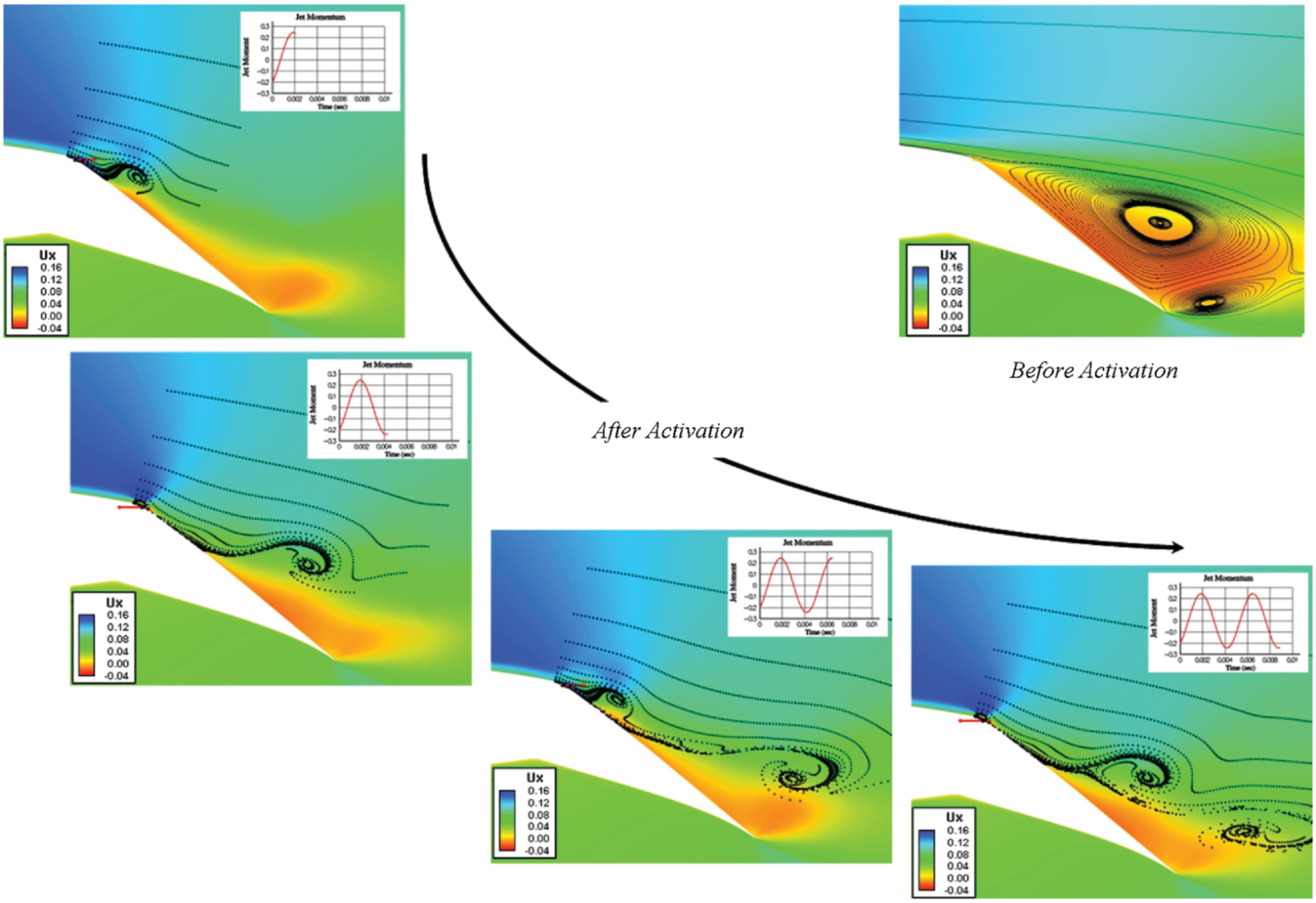

Fig. 3 Short time-scale flowfield description in the limit-cycle stage for $\delta_{\text{flap}} = 25$ deg, $\alpha = 11$ deg (u_x contours).

element section with the AFC application at the hinge line for the 25 deg flap deflection is shown in Fig. 7. Because viscous effects significantly reduce the lifting capability, especially with flaps deflected, an inviscid analysis is used to determine the theoretical upper limit of the lift production of the airfoil. The corresponding inviscid lift curve is also shown in Fig. 7. Obviously, it is desirable to devise an AFC approach that will farther mitigate the viscous effects and achieve lift close to the inviscid level. Equivalently, the inviscid lift level can be viewed as a design objective for a highly effective AFC implementation.

In the current approach, a set of actuators is employed in a way that maximizes their cumulative effectiveness. An array of five actuators is used, in which the individual ports are placed at equal intervals within the flap between the hinge line and a station upstream of the trailing edge as shown in Fig. 8. The actuators are positioned such that their respective orifice axes form a 20 deg angle relative to the local upper surface of the flap. Actuation patterns with sinusoidal signals at $f = 217$ H_z, $C_\mu = 0.015$ are employed. Collectively, the active set of actuators provides mixing in the viscous shear flow in regions where a discrete corrective application is warranted, resulting in an overall improved high-lift performance.

The flow structure in the aft portion of the airfoil for a freestream Mach number of 0.09 and an 11 deg angle of attack is shown in Fig. 9. The baseline viscous solution is presented in the upper left corner, showing a large pocket of flow reversal. In contrast, the flow structure for an inviscid flow is also shown for reference. Indeed, this is an unrealistic situation that represents an ideal flow without viscous losses as demonstrated by the smooth and highly curved streamlines. It will be shown in the following discussion that this case provides a useful yardstick by which to assess the efficiency of distributed AFC.

The flowfields obtained with different modes of flow control are shown in the row of plots at the bottom of Fig. 9, starting with a single port application (port 1) on the left-hand side (similar to the case presented in Fig. 3). The effectiveness of the various AFC modes is gauged by the lift augmentation, drag reduction, and suppression of flow reversal. The unsteady flow is described by traces of particles over a time interval corresponding to two actuation cycles. Equivalently, this can be viewed as snapshots at 0.0092 s after the start of the particle release. The first port located close to the hinge line where the baseline separation originates is effective in reducing the region of flow reversal in the front part of the flap. The domain of flow reattachment can be viewed as the range of influence of port 1. The improved flow translates to an increment of 0.65 in the time-averaged lift coefficient relative to the baseline.

The next flow control application uses port 3 in the middle of the flap. Despite the local flow reattachment realized downstream of the port, the separation bubble originates at the hinge line just like in the baseline case and without effective flow turning at the flap. The excitation in this case does not have a meaningful impact on the global separation pattern and results in a modest lift gain. The third flow control mode consists of the simultaneous actuation of ports 1 and 3 (denoted ports 13). This results in a favorable momentum cascading effect whereby the location of port 3 at the end of the range of influence of port 1 proves very effective. In the last flow control mode shown in Fig. 9, all five ports are used (12345). Here, a phase shift of 180 deg has been used between the odd numbered ports (1, 3, and 5) and the even numbered ports (2 and 4). The simultaneous jet pulsation imparts momentum to the flow in the flap region. The particle traces illustrate a unique flow structure in which the original separation bubble has been effectively altered to a predominantly attached flow. The cumulative effect provided by the multiple ports results in a lift gain of 1.33 relative to the baseline, and it represents more than twice the gain realized with the single actuation at port 1. Further confirmation of the effectiveness of distributed actuation is demonstrated by the resemblance of this flow control mode to the smooth and regular flow structure in the inviscid case. Also, the lift is close to the upper-limit-ideal lift level obtained with the inviscid case.

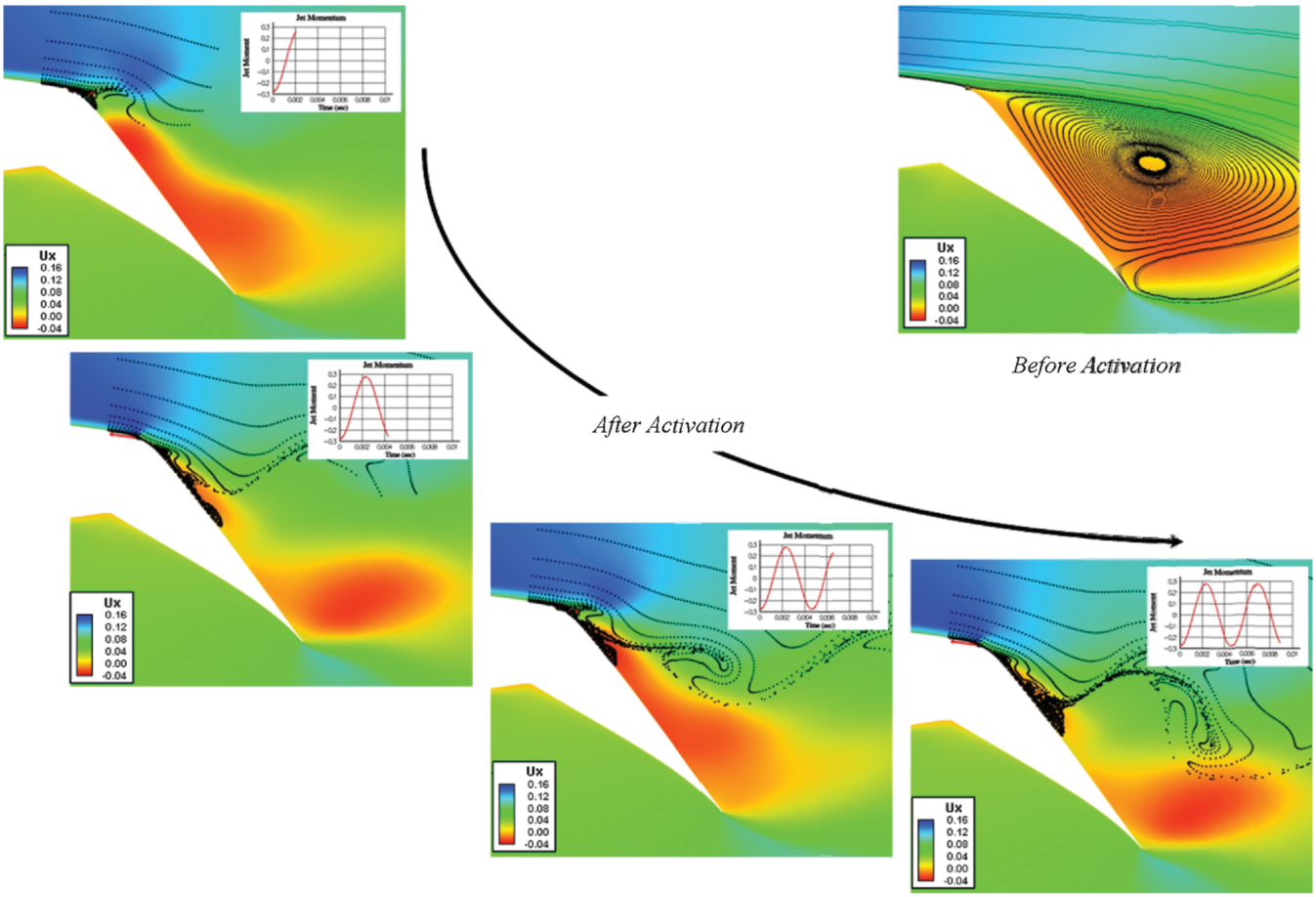

Fig. 4 Short time-scale flowfield description in the limit-cycle stage for $\delta_{\text{flap}} = 40$ deg, $\alpha = 11$ deg (u_x contours).

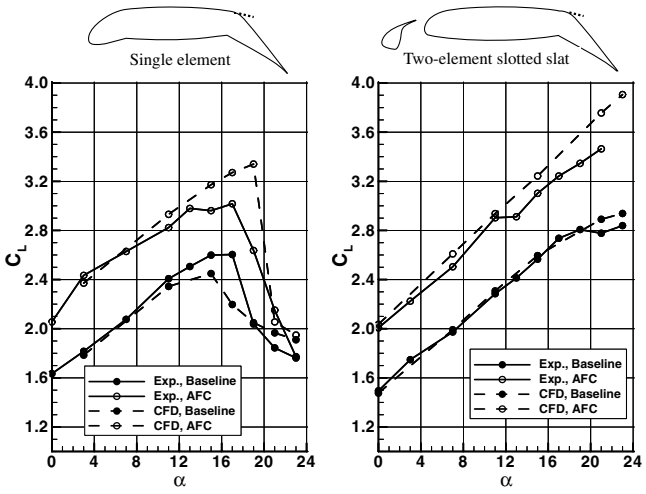

Fig. 5 Comparison between the experimental data and computational results for $\delta_{\text{flap}} = 40$ deg.

Before the aerodynamic performance of the distributed AFC is discussed, a note on the improvements in the estimated drag is in order. In the following discussion, the estimated forces are based on two-dimensional simulations. Consequently, the induced drag is not accounted for because this drag component is an artifact of flow past finite wings. Therefore, the drag and L/D predictions in the following discussion should be appropriately interpreted. At this point, it is emphasized that in the current approach the AFC directly impacts the profile drag. Although the profile drag constitutes a significant part of the total airplane drag, the distributed AFC can also be used to tune the wing load to minimize the induced drag component.

The results shown in Fig. 9 are presented in the context of a systematic buildup of lift, drag, and L/D for a distributed AFC in Fig. 10. The force parameters are plotted as a function of port number. Because the ports are placed at equal intervals, the abscissa can be viewed as the streamwise coordinate along the flap between port 1 and 5. For the convenient interpretation of the results, the baseline values are included at the 0 station. Three modes of application are being considered. First, the successive actuation of the flow control is shown with the open circles. These results indicate that the AFC application in the forward region of the separation bubble is very effective. The efficiency diminishes when the flow control is applied at downstream locations, with almost zero gain for port 5. In the second set of AFC patterns, the ports are activated in an additive fashion starting with port 1 and sequentially adding the subsequent ports (12, 123, 1234, and 12345). This set is described with the dark circles illustrating substantial gains relative to the individual port 1. The addition of the flow actuation toward the trailing edge provides incrementally smaller gains, with the lift approaching the inviscid level. The third set of control applications is similar to the second additive pattern but uses every other port. This set includes the 13 and 135 port groupings. Interestingly, these patterns are almost as effective as the denser AFC pattern because the range of influence of port 1 is comparable to approximately twice the distance between the ports. In particular, the similar slopes of the respective curves in the ranges 123–12345 and 13–135 imply that port 4 is ineffectual when its neighbors 3 and 5 are activated. For example, the three actuators, 135, generate 88% of the lift gain obtained with the five actuators, 12345.

The aerodynamic performance parameters of the distributed AFC are shown in Fig. 11. Here, the performance envelope is presented for the 3–15 deg angle-of-attack range. The red dashed line indicates the envelope of actuator 1 and the red solid line denotes the expanded

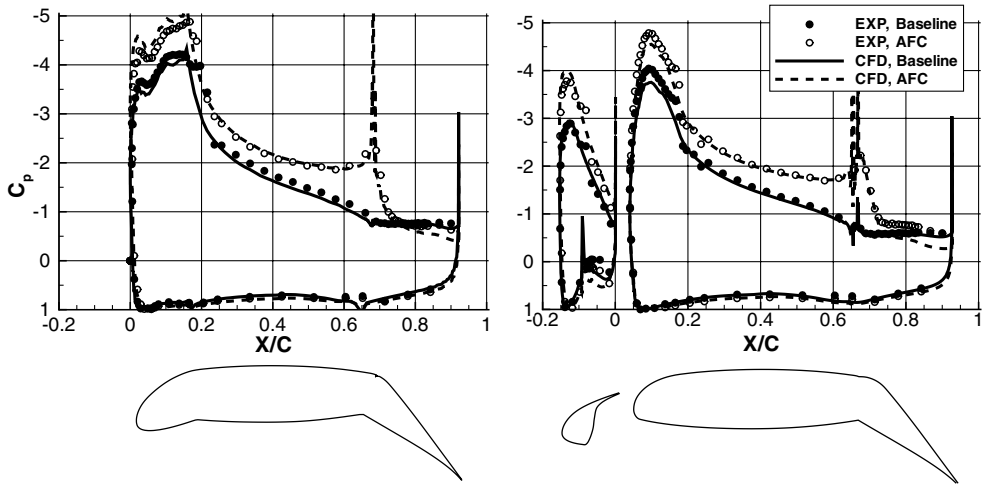

Fig. 6 Time-averaged pressure distributions for $\delta_{\text{flap}} = 40$ deg, $\alpha = 11$ deg.

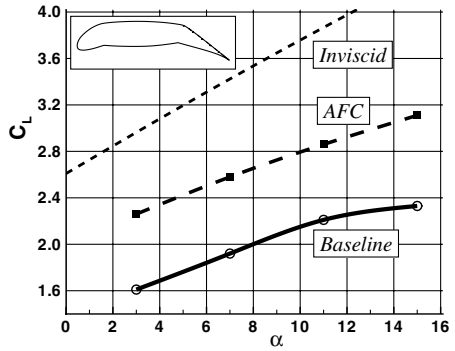

Fig. 7 Lift increment due to the application of flow control at the flap hinge line, $\delta_{\text{flap}} = 25$ deg.

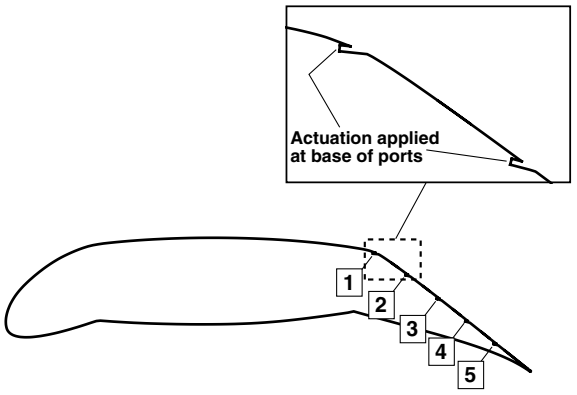

Fig. 8 Distributed flow control on the upper surface of the flap.

domain due to the distributed actuation. Although the control provided by port 1 is large, the multiple actuation mode results in further substantial gains in the lift and reduction of drag. In particular, the lift obtained with pattern 12345 is quite close to the inviscid levels, especially at the lower flow incidence (refer also to Fig. 7). The advantage of distributed actuation is also exhibited in the drag polar. For example, at $C_L \approx 2.85$ the 12345 actuation mode results in an approximately 75% reduction in drag relative to the level obtained with the single actuator.

The time-averaged pressure distributions and off-surface streamwise component of the velocity for the sequential additive applications at $\alpha = 11$ deg are shown in Fig. 12. In the time-averaged sense, the AFC augments the load on the airfoil, and the multiple patterns 123, 1234, and 12345 result in the flow reattachment over the entire flap. The small-scale pockets of flow reversal that form as a result of these actuation modes enable the recontouring of the mean flow to better conform to the airfoil even for large flap deflections. This streamlining effect was mentioned earlier; the resemblance of the flow structure of the 12345 pattern to the inviscid flow was pointed out in reference to Fig. 9. The effective turning of the mean flow and the ensuing loading over the entire airfoil due to increased circulation is illustrated in Fig. 13.

At this point, it is instructive to evaluate the sensitivity of select actuation modes on aerodynamic performance. A series of simulations revealed that added performance improvements can be realized with several variants of distributed AFC. For example, the effect of the AFC synchronization is shown in Fig. 14, in which the in-phase flow control is compared with the out-of-phase additive patterns in Fig. 10. Relative mild improvement is realized when in-phase actuation is applied at more than two ports. Figure 15 shows another variant in which ports 2 and 4 use the nominal harmonics of 217 Hz and ports 1, 3, and 5 use four times the nominal frequency. This is compared with the case in which the nominal frequency of 217 Hz is applied to all ports in Fig. 10, showing a modest lift increment. The examples in Figs. 14 and 15 demonstrate that the aerodynamic performance is not very sensitive to variations in actuation parameters. This is an important point, implying that there is no need for a narrow "point design" with respect to actuation parameters for attaining a given lift level. Instead, actuation parameters might be important with regard to other design disciplines as described in Sec. V.

V. Practical Implementation of Distributed Flow Control

The flexibility provided by varying actuation parameters without adversely affecting the aerodynamic performance has very important implications with respect to the practical integration of the AFC. The unique attributes of distributed flow control make this technology particularly attractive for airframe integration. Some of the most relevant design considerations are as follows:

1) Performance envelope: The multitude of port arrangements provides a broad performance envelope. Meaningful versatility can be obtained (i.e., choices of C_L and L/D) depending on the flight condition. This facilitates a practical multipoint design for the range of takeoff, approach, and landing conditions (see Fig. 11).

2) Wing load: The select application of flow control can be exploited for managing the wing load. This presents a palatable option for designing to specific induced drag levels, depending on the flight conditions. More specifically, for takeoff, a near elliptical span load distribution ensures a low level of induced drag. On the other hand, during landing, a distribution with a higher load in the inboard wing region is desired to produce higher drag levels.

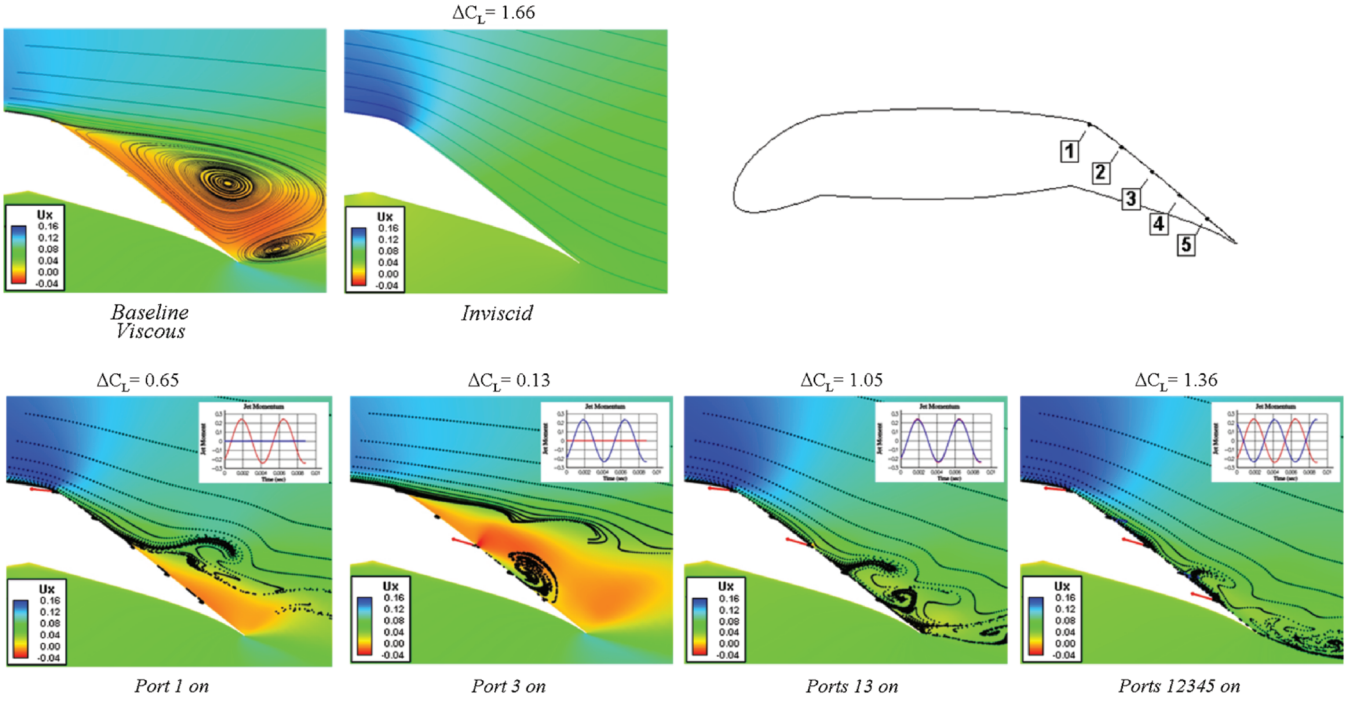

Fig. 9 Flow structure for various actuation modes, $\delta_{\text{flap}} = 25$ deg, $\alpha = 11$ deg (u_x contours).

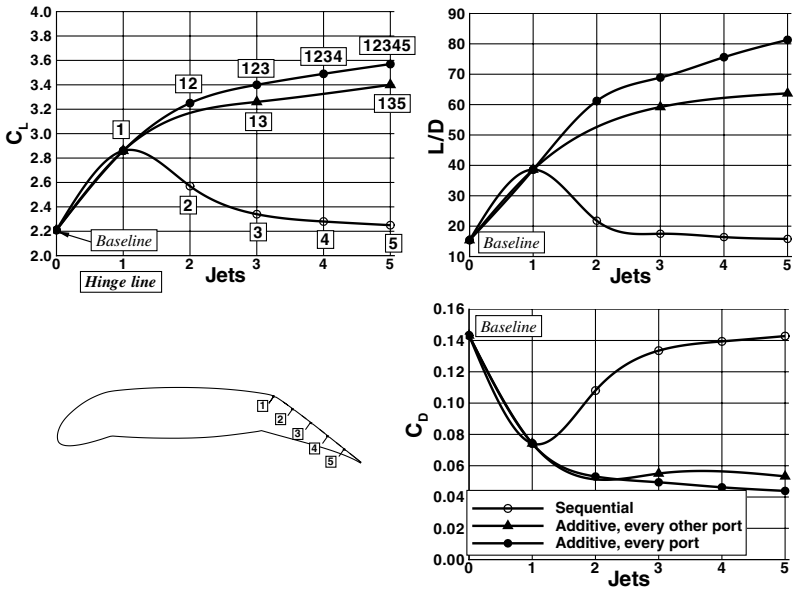

Fig. 10 Buildup for distributed flow control, $\alpha = 11$ deg.

3) Stability and control (S&C): The wing load can be tailored by using the AFC for airplane S&C, replacing or reducing the control surface usage.

4) Structural excitation and implications on structural fatigue: Pulsed excitation results in unsteady forces and moments with significant amplitudes. These perturbations are detrimental to the structural integrity of the airplane, and the distributed flow control has practical implications with respect to structural fatigue. This point is illustrated in Fig. 16, which shows the transitory lift buildup for the additive patterns 1, 12, 123, 1234, and 12345 described in Fig. 10. Airfoil lift is plotted from the start of the actuation until the limit cycle of each pattern is reached. The fluctuating lift levels strongly depend on the activation patterns; when an even number of ports are employed, an offsetting mechanism occurs resulting in smaller force oscillations. Likewise, the fluctuations relative to the respective nominal lift are shown in the inset, indicating that depending on the mode of actuation amplitudes of up to 5% of total lift are experienced by the airfoil. It is thereby desirable to employ actuation parameters such that the resultant forces and moments are free of large fluctuations.

5) Acoustics: AFC actuation parameters can be used for noise abatement. Because separated flow is one of the major sources of airplane noise, the mere reduction in flow separation provided by the AFC will result in reduced noise levels. However, another potential noise source is associated with the operation of the AFC itself. With the proper design of the port layout and the pulse modulation of individual actuators, it is possible to achieve noise suppression within acceptable levels.

The wide range of AFC attributes implies that an integrated approach to aircraft design that encompasses many disciplines,

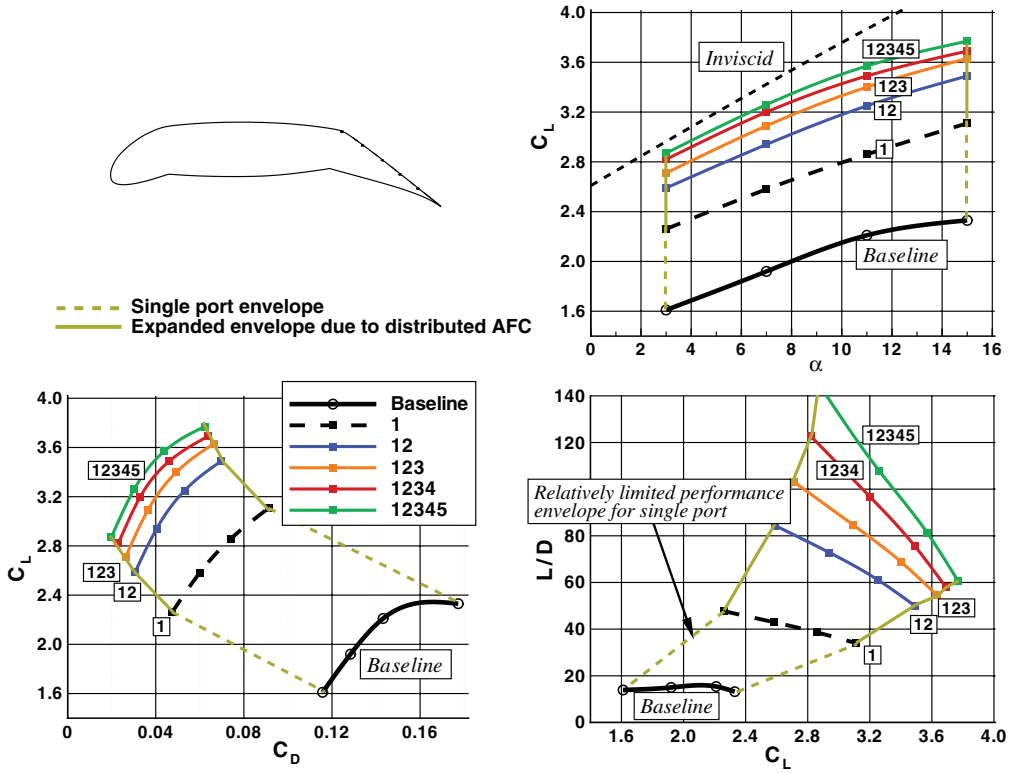

Fig. 11 Aerodynamic performance of distributed flow control.

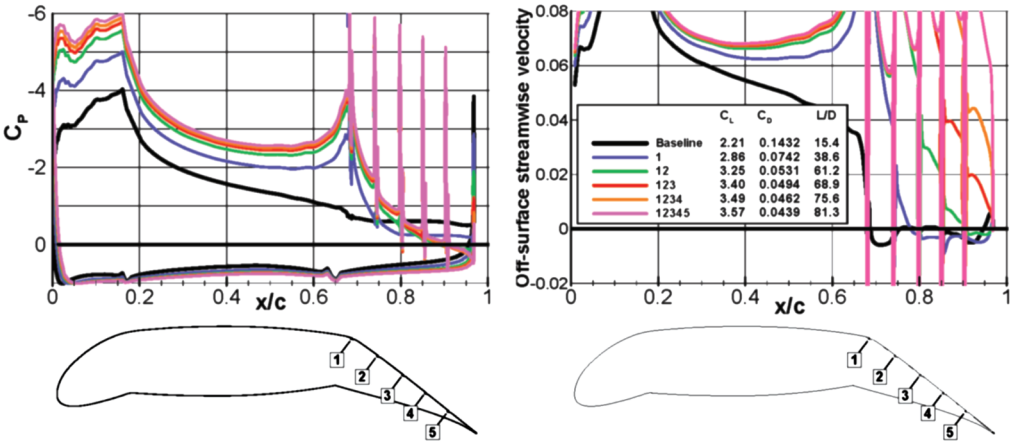

Fig. 12 Time-averaged *Cp* and off-surface velocity for the set of additive flow patterns, $\alpha = 11$ deg.

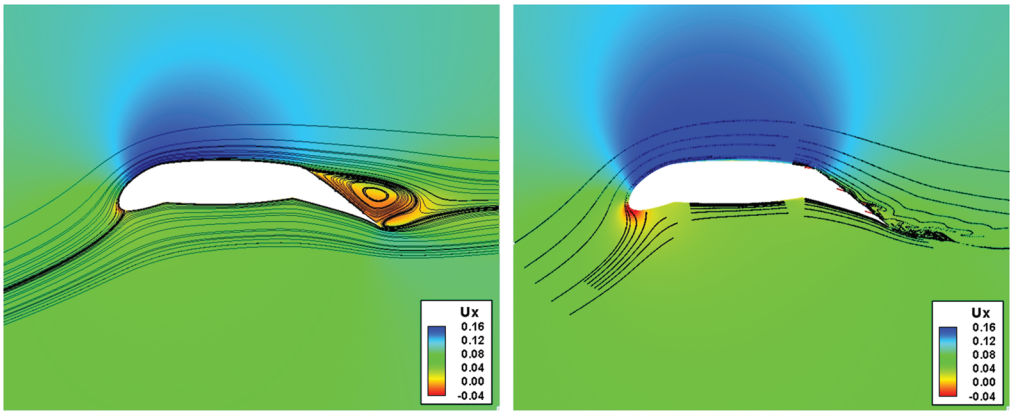

Baseline AFC (*12345*)

Fig. 13 Global flow structure illustrating the streamlining due to the flow control application for $\delta_{\text{flap}} = 25$ deg, $\alpha = 11$ deg (u_x contours).

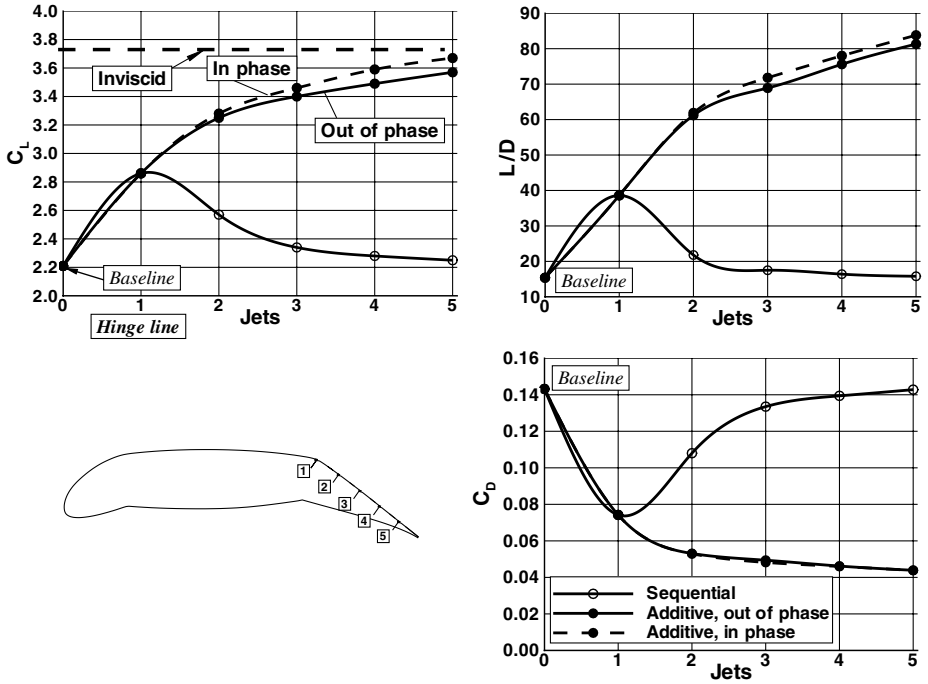

Fig. 14 Synchronization effects for the 12345 pattern, $\alpha = 11$ deg.

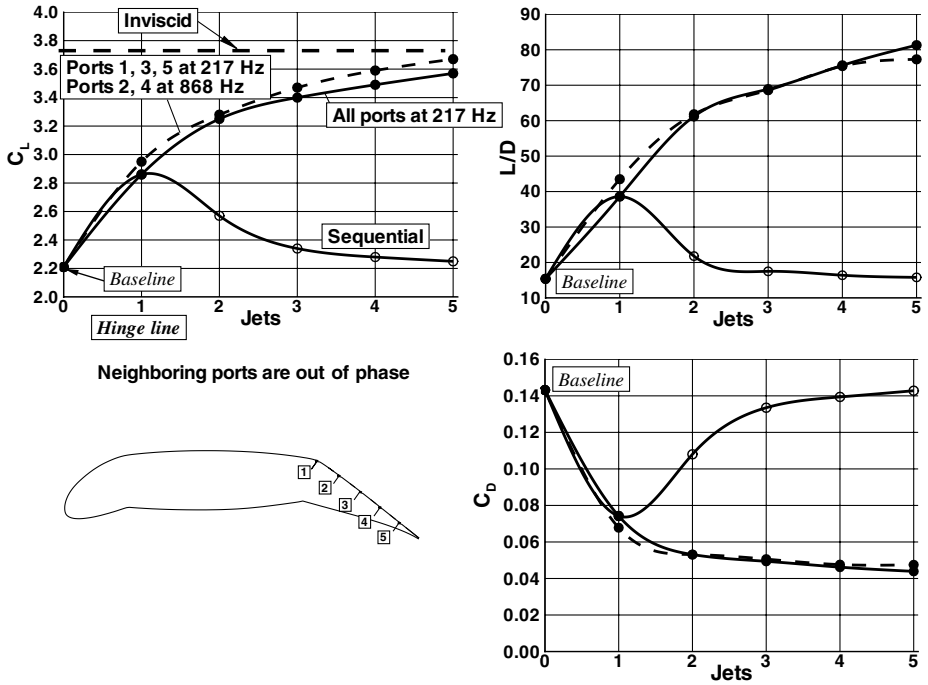

Fig. 15 Frequency effects for the 12345 pattern, $\alpha = 11$ deg.

including structures, noise, S&C, aerodynamics, power requirements, and systems integration, is indispensable. This versatility greatly enhances the practical appeal of distributed flow control for real-world designs.

VI. Conclusions

A computational process for the simulation of AFC flows has been developed. Validation with experimental data for two-dimensional applications indicates that the analysis is valid in the linear lift range. The agreement deteriorates with increased flow incidence, with major discrepancies near maximum lift conditions. Possible sources of inconsistencies at maximum lift are a) the deficiency of the computational tool in modeling highly separated flows, b) the excessive wall interference in the experiment, and c) the approximate AFC signal shape used in simulations.

The computational tool was then used to devise techniques for substantially increasing the performance of a high-lift system. Because of the broad range of possible actuation parameters, a series of numerical experiments using various ports and actuation modes was used to bring potential AFC implementations into sharper focus. An important element of the design process is the ability to establish aerodynamic design goals to clarify the options available when considering the complexity and effectiveness of AFC systems. For this purpose, the inviscid lift level has been used as the yardstick by which the efficiency of the AFC can be conveniently gauged in the

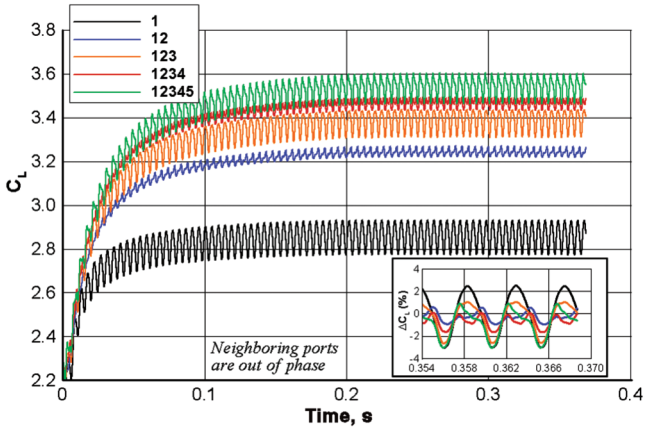

Fig. 16 Transitory lift development, additive patterns, $\alpha = 11$ deg.

linear lift range. According to the simulations, when the actuators are properly placed, the flow excitation has a favorable effect on the state of the viscous layer. For separated flow cases at a high angle of attack, the separation bubble morphs into small pockets of flow reversal. In a time-average sense, the excitation can be viewed as a mechanism of flow reattachment whereby the lift close to the inviscid level can be achieved. The efficiency of active control is realized even for nonseparated flows at a modest flow incidence in which the application engenders a high-momentum viscous flow with a reduced propensity for separation. The systemic impact of distributed AFC results in a substantial gain in lift and drag reduction over the practical range of angles of attack. In addition to the profound aerodynamic benefits, AFC technology offers a pathway toward higher efficiencies in a range of airplane design disciplines.

References

[1] Garner, P. L., Meredith, P. T., and Stoner, R. C., "Areas for Future CFD Development as Illustrated by Transport Aircraft Applications," AIAA Paper 1991-1527, 1991.

[2] Washburn, A. E., Gorton, S. A., and Anders, S., "A Snapshot of Active Flow Control Research at NASA Langley," AIAA Paper 2002-3155, 2002.

[3] Sellers, W. L., III, Jones, G. S., and Moore, M. D., "Flow Control at NASA Langley in Support of High-Lift Augmentation," AIAA Paper 2002-6006, 2002.

[4] Gorton, S. A., Jenkins, L., and Allan, B., "Active Flow Control on a Boundary-Layer-Ingesting Inlet," AIAA Paper 2004-1203, 2004.

[5] Wygnanski, I., "The Variables Affecting the Control of Separation by Periodic Excitation," AIAA Paper 2004-2505, 2004.

[6] Tilmann, C. P., Kimmel, R. L., Addington, G. A., and Myatt, J. H., "Flow Control Research and Applications at the AFRL's Air Vehicles Directorate," AIAA Paper 2004-2622, 2004.

[7] Anders, S. G., Sellers, W. L., III, and Washburn, A. E., "Active Flow Control Activities at NASA Langley," AIAA Paper 2004-2623, 2004.

[8] Kibens, V., and Bower, W. W., "An Overview of Active Flow Control Applications at the Boeing Company," AIAA Paper 2004-2624, 2004.

[9] Vukasinovic, B., Brzozowski, D., and Glezer, A., "Separation Control over a Surface-Mounted Hemispherical Shell," AIAA Paper 2005-4878, 2005.

[10] Smith, D. R., Amitay, M., Kibens, V., Parekh, D., and Glezer, A., "Modification of Lifting Body Aerodynamics Using Synthetic Jet Actuators," AIAA Paper 1998-0209, 1998.

[11] Chatlynne, E., Rumigny, N., Amitay, M., and Glezer, A., "Virtual Aero-Shaping of a Clark-Y Airfoil Using Synthetic Jet Actuators," AIAA Paper 2001-732, 2001.

[12] Amitay, M., Smith, D. R., Kibens, V., Parekh, D. E., and Glezer, A., "Aerodynamic Flow Control over an Unconventional Airfoil Using Synthetic Jet Actuators," *AIAA Journal*, Vol. 39, No. 3, 2001, pp. 361–370.

[13] Greenblatt, D., and Wygnanski, I., "Effect of Leading-Edge Curvature on Airfoil Separation Control," *Journal of Aircraft*, Vol. 40, No. 3, 2003, pp. 473–481.

[14] Gilarranz, J. L., Traub, L. W., and Rediniotis, O. K., "A New Class of Synthetic Jet Actuators—Part 2: Application to Flow Separation Control," *Journal of Fluids Engineering*, Vol. 127, March 2005, pp. 377–387.
doi:10.1115/1.1882393

[15] Hassan, A., "A Two-Point Active Flow Control Strategy for Improved Airfoil Stall/Post-Stall Aerodynamics," AIAA Paper 2006-0099, 2006.

[16] Spalart, P., Hedges, L., Shur, M., and Travin, A., "Simulation of Active Flow Control on a Stalled Airfoil," *Flow, Turbulence and Combustion*, Vol. 71, 2003, pp. 361–373.
doi:10.1023/B:APPL.0000014925.91304.42

[17] Melton, L. P., Yao, C. S., and Seifert, A., "Application of Excitation from Multiple Locations on a Simplified High-Lift System," AIAA Paper 2004-2324, 2004.

[18] Schatz, M., Thiele, F., Petz, R., and Nitsche, W., "Separation Control by Periodic Excitation and Its Application to a High Lift Configuration," AIAA Paper 2004-2507, 2004.

[19] Kiedaisch, J., Demanett, B., and Nagib, H., "Active Flow Control Applied to High-Lift Airfoils Utilizing Simple Flaps," AIAA Paper 2006-2856, 2006.

[20] Buning, P. G., Chiu, I. T., Obayash, S., Rizk, Y. M., and Steger, J. L., "Numerical Simulation of the Integrated Space Shuttle Vehicle in Ascent," AIAA Paper 1988-4359, 1988.

[21] Galbraith, C. M., "Numerical Simulations of a High-Lift Airfoil Employing Active Flow Control," AIAA Paper 2006-0147, 2006.